Environmental Science Processes & Impacts

Accepted Manuscript

Results of this study suggest that built-up area and bare land can increase air pollution stronger in May than that in October, while forest and water have totally opposite effects. The difference in cropland impact on air pollution reveals that green coverage and human activity also influences the AOD patterns. This work will enable us to better understand the processes involved in the effects of land use variations on the AOD for policy making and land use planning.

Exploring the effects of landscape structure on Aerosol Optical Depth (AOD) patterns using GIS and HJ-1B images

Luping Ye[1], Linchuan Fang[2]*, Wenfeng Tan[1], Yunqiang Wang[3], Yu Huang[4]

1. State Key Laboratory of Soil Erosion and Dryland Farming on the Loess Plateau, Institute of Soil and Water Conservation, Chinese Academy of Sciences and Ministry of Water Resources, Yangling 712100, China
2. State Key Laboratory of Soil Erosion and Dryland Farming on the Loess Plateau, Northwest A&F University, Yangling 712100, China
3. State Key Laboratory of Loess and Quaternary Geology, Institute of Earth Environment, Chinese Academy of Sciences, Xi'an, Shaanxi 710075, China.
4. Wuhan Environmental Protection Sciences Research Institute, Wuhan 430000, China.

*Corresponding author. Tel: +86-29-87671033. Fax: +86-27-87280670. E-mail: flinc629@hotmail.com (Linchuan Fang)

Abstract

A GIS approach and HJ-1B images were employed to determine the effect of landscape structure on aerosol optical depth (AOD) patterns. Landscape metrics, fractal analysis and contribution analysis were proposed to quantitatively illustrate the impacts of land use on AOD patterns. The high correlation between the mean AOD and landscape metrics indicates that both the landscape composition and spatial structure affects the AOD pattern. Additionally, the fractal analysis demonstrated that the densities of built-up area and bare land decreased from the high AOD centers to the outer boundary, but those of water and forest increased. These results reveal that built-up area is the main positive contributor to air pollution, followed by bare land. Although bare land had a high AOD, it made a limited contribution to the regional air pollution due to its small spatial extent. The contribution analysis further elucidated that built-up area and bare land can increase air pollution more strongly in spring than in autumn, whereas forest and water have a completely opposite effect. Based on a fractal and contribution analysis, the different effects of cropland are ascribed to the greater vegetation coverage from farming activity in spring than in autumn. The opposite effect of cropland on air pollution reveals that green coverage and human activity also influences AOD patterns. Given that serious concerns have been raised regarding the effects of built-up area, bare land and agricultural air pollutant emissions, this study will add fundamental knowledge of the understanding of the key factors influencing urban air quality.

Keywords: Aerosol Optical Depth pattern; Landscape structure; Fractal analysis; Contribution; HJ-1B; Wuhan

1 Introduction

In many developing countries, including China, air quality has been experiencing a progressive degradation as a consequence of rapid development. Urban air pollution is increasing rapidly with the increase in urban populations, the number of automotive vehicles, the use of fuels with poor environmental performance [1] and the spatial distribution of different land use and land cover classes [2-4]. Numerous studies correlate severe air pollution issues with increasing morbidity and even death over the past century [5]. With a large total population living in urban areas, it is necessary to analyze and address the key points influencing air quality.

The aerosol optical depth (AOD), which represents the integrated extinction of the total column of aerosols, is one of the most important indicators related to air quality [6]. It plays a critical role in the Earth Radiation Budget and is commonly measured from satellites. Remote sensing data have provided a powerful and effective method to monitor the temporal and spatial variability of aerosol distribution around the world, allowing us to analyze their influence and optical properties [7-9]. The dark dense vegetation method (DDV), which was pioneered by Kaufman et al. [10], has been widely applied to AOD retrieval. This method relies primarily on the low reflectance of dark land targets in the red and blue spectral regions. For a bright surface, the common classic methods are the Deep Blue algorithm [11, 12] and the structure function method (SFM) [13]. It is challenging but valuable work to retrieve high-resolution AOD information to assess air pollution and other physical parameters using remote sensing images [14]. This experiment conducts an investigation on the basis of HJ-1B images, which are dedicated to the environment and disaster monitoring in China. The NDVI (Normalized Differential Vegetation Index) thresholds test, which is a common method of retrieving aerosol inversion [14, 15], is utilized to identify the dark pixels and calculate the AOD.

Regional air pollution patterns in urban areas are correlated with the land use type and pattern, which mainly results from natural land cover being replaced by manmade sources of pollution [2]. Furthermore, the conversion of green fields (including forest, grassland and cropland) to urban areas always leads to an increase in emissions of air pollutants [16-18]. The built-up areas are related to the sources of a variety of air pollutant emissions, in addition to other pollution problems, such as noise pollution, photochemical smog, water pollution and acid rain. The urban pollution intensity increase with land use density, which has a tendency to increase towards the center of urban areas. Hence, the concentrations of air pollutants form a decreasing gradient from urban areas to rural surroundings [2]. Several studies have explored the land use type and the effects of land use change on urban air pollution in various regions [19, 20]. For example, Romero et al. [18] studied the relationship between land use change and air pollution, which indicated higher air pollution in the winter and in the parts of the city where there was bare land, industries and deforested slopes.

Weng and Yang [2] analyzed how urban growth and connected land use/cover changes altered the regional air pollution pattern. They found that the spatial distributions of air pollutants were positively related to the density of the urban built-up area. Superczynski and Christopher [21] explored the effects of land use and land cover on air quality, which showed a moderate-to-strong relationship between Particulate Matter$_{2.5}$ ($PM_{2.5}$) data and built-up area surrounding monitoring sites.

In Wuhan, air pollution has become more and more serious in recent decades because of rapid land use changes, such as the conversion of forest, suitable agricultural lands, water and natural conservation areas to buildings, roads and residences [22]. Therefore, this investigation combines landscape metrics and fractal analysis with contribution analysis to explore the effects of land use types and landscape structure on the AOD patterns in Wuhan. Land use patterns have commonly been characterized by landscape metrics [23, 24]. In addition, fractal analyses have been widely adopted to analyze the urban geography phenomenon [25-27]. Our objective is to explore how seasonal variations in land use and the spatial configuration have affected variations in the AOD pattern. In addition, the contributions of each land use change to the AOD are calculated. The understanding of regional AOD properties obtained in this study will add fundamental knowledge to land use planning and environmental management to reduce the adverse environmental effects.

2 Material and methods

2.1 Study Area and data collection

Wuhan (also known as stove city), which is situated at the confluence of the Yangtze River and the Han River, is located between 113°41′ and 115°05′ E longitude and between 29°58′ and 31°22′ N latitude (Fig. 1). With a population of 10.12 million, of which approximately 5.55 million of them reside in urban core districts, and with total area of 888 km^2, it ranks fourth in population in China. This city has a subtropical monsoon climate with an average annual temperature of 16.6°C, with the lowest temperature in January (averaging 3.7°C) and the highest temperature in July (averaging 25.4°C). Wuhan includes many industries (such as steel production, chemical plants and power plants, etc), where production and transportation emit a large quantity of polluting gases and aerosol particles. The major sources of atmospheric pollution in Wuhan are motor vehicles, the utilization of coal and industrial processes.

The HJ-1B satellite was launched at 11:25 a.m. on September 6, 2008, which carries two CCD cameras and one IRS camera (Table 1). With a high spatial resolution of 30 m and a two day revisit cycle (jointly used with HJ-1A satellite) [28], it can achieve all-weather and all-day monitoring of environmental changes in China. To quantitatively analyze the effects of landscape structure on AOD patterns, nineteen cloud-free HJ-1B images (Mar. 19, 2010; May 24, 2010; Oct. 22, 2010; Oct. 31, 2010; Mar. 29, 2011; Mar. 27, 2011; May 19, 2011; Oct. 8, 2011; Oct. 18, 2011; Mar. 26, 2012; May 10, 2012; Oct. 2, 2012; Oct. 17, 2012; Mar. 8, 2013; Apr. 7, 2013; May 11, 2013; Sep. 19, 2013; Oct. 12, 2013 and Nov. 25, 2013) were chosen. To perform a landscape analysis, this study took a subset of a 50×50 km sample plot, which was carefully selected to represent the city landscape structure (Fig. 1).

2.2 Image Pre-processing

The pre-processing of the HJ-1B images was performed using ERDAS image 9.1 and ENVI 5 software. To convert the DN (Digital Number) to radiance, the images should first be radiometrically corrected. Fig. 2 shows the general framework of the assessment of urban air pollution patterns. Before interpreting the HJ-1B images, there was a land use ground reconnaissance at first. And the general understanding of Wuhan's land use situation was obtained. In the process of interpretation, a comprehensive analysis of statistics and graphics was used to identify land use features. Then, bands 2, 3, and 4, which were deemed to be most effective in discriminating land use types, were selected for classification. The classification categories include cropland, built-up area, forest, bare land and water. Given that each land use type may contain various objects, an unsupervised clustering method with an ISODATA classifier was utilized to classify the HJ-1B images in advance. The maximum likelihood classification was also employed to further extract the classification information. The land use classification results are shown in Fig. 3. Thereafter, a random sampling method that incorporated reference data was performed to examine the accuracy of classification. The sampling points were selected from each land use type and taken across the study area. These reference data were obtained from field investigations. Given that there were minor changes occurring on the land cover and land use in a short time, the land use maps of May 11, 2013 and Oct. 12, 2013 with a spatial resolution of 30 × 30 m were selected to represent the land use spatial distributions in spring and autumn, respectively. The overall accuracy of the classification was approximately 91.02 percent (May 11, 2013), and 90.41 percent (Oct. 12, 2013).

2.3 The calculation of the aerosol optical depth (AOD)

The DDV method can be imported to retrieve the AOD from images [29]. Based on the Look Up Table (LUT), the AOD of a cloud-free land pixel is retrieved. To quantitatively analyze the correlation between the variations of air pollution patterns and land use types, the mean AODs were calculated for representing the AODs in spring and autumn (see Supporting Information). Given that the CCD spatial resolution (30 m) can bring about the effect of topographic relief, causing a reduction in the SNR (Signal Noise Ratio) and the efficiency, the CCD images are re-sampled to a 300 m resolution. The retrieval of a 300×300 m resolution AOD from the HJ-1B CCD images includes these steps as follows.

Suppose that the atmosphere is horizontally homogeneous and vertically non-homogeneous, the apparent reflectance at the top of the atmosphere (TOA) can be expressed as follows [30]:

$$\rho_{TOA} = \rho_a(\mu_s, \mu_v, \phi) + \frac{T(\mu_s)T(\mu_v)\rho(\mu_s, \mu_v, \phi)}{1 - s\rho(\mu_s, \mu_v, \phi)} \quad (1)$$

where $\mu_s = \cos\theta_s$; $\mu_v = \cos\theta_v$; θ_s and θ_v are the solar zenith and satellite zenith, respectively; ϕ is relative azimuth angle; T is atmospheric transmissivity; ρ_a is atmospheric reflectivity; s is atmospheric albedo; and $\rho(\mu_s, \mu_v, \phi)$ is surface emissivity. Then, the AOD retrieval was achieved using a LUT, which was built based on 6S (Second Simulation of the Satellite Signal in the Solar Spectrum). 6S is a computer code that can accurately simulate plane observations and the signal observed by the satellite sensor, etc. [30]. The LUT contains pre-computed atmospheric optical properties (s, ρ_a, T), which results from different input parameters. As for the AOD, its viewing geometry includes θ_s, θ_v and ϕ. Given that the difficulty in using HJ-1B images to retrieve the AOD is due to the lack of a short infrared band, the NDVI was imported to extract the dark pixels. Then, the DDV method was used to retrieve the AOD.

$$NDVI = (\rho_4 - \rho_3)/(\rho_4 + \rho_3) \quad (2)$$

where ρ_4 is the reflectance of the near-infrared band; and ρ_3 is the reflectance of the red band. The pixels with a $NDVI_v > 0.3$ are recognized as dark pixels [31]. Based on the aforementioned steps, the AOD map was derived for the study area and is shown in Fig. 4.

2.4 Calculation of landscape metrics

Urban air pollution patterns could be related to land use type and land use change [2, 21]. In the past few decades, there are a large number of studies that have developed and widely applied landscape metrics to describe landscape patterns [32-35] and to correlate landscape patterns to ecological processes [36, 37]. These metrics are composed of two general types that analyze the landscape composition and spatial configuration. The composition metrics describe the existence and amount of various land use types within the entire landscape. The spatial configuration metrics describe the spatial features. At first, there were twelve class-based and fourteen landscape-based metrics that were commonly used to associate the AOD with landscape patterns. However, given that many of them were highly correlated and choosing uncorrelated landscape metrics was an important principle, six class-based metrics and five landscape-based metrics were finally selected. These landscape metrics are given in Table 2. They were chosen to provide complementary information of the landscape structure both the landscape composition and the spatial configuration.

We divided the study area into 25 subplots of 10×10 km in size to develop a statistical relationship. FRAGSTATS, the spatial pattern analysis software [38], was utilized to calculate the landscape metrics of each land use type and the total landscape. When computing the class-based metrics for a type, all other land use types within a subplot would be masked out as background. For the landscape-based metrics, all land use types within each subplot must be taken into account. Then, the mean AODs of each land use type and subplot were calculated to further analyze their correlation with landscape metrics using Pearson's correlation coefficients. A two-tailed Student's t-test was used to determine the significance of each correlation coefficient.

2.5 Fractal analysis

The radius dimension of the fractal dimension was first proposed by Frankhauser and Sadler [39] and incorporated into the analysis of the spatial patterns of urban land use by White and Engelen [40]. The fractal analysis is mainly used as an effective way to depict spatial features of land surface temperature (LST). To further understand the relationship between variations in the AOD and different land use types, the radius dimension was imported to analyze the variation over land use types associated with AOD patterns. First, both the extraction of the analysis center (Fig. 5) and the increment of a buffer radius needed to be analyzed. Then, the density slice was utilized to extract the high AOD centers with ENVI 5 software. Given that a limited range of each center was affected by air pollution, only 1.1% of the pixels were deemed to be the center of the high AOD. Another key analysis was the ascertainment of the buffer radius and the increment value. As a result of the involvement of a large amount of data, it was impractical to perform a fractal analysis using too small radius increment for the study area. It was also meaningless to adopt a wide increment because there would not be a sufficient number of samples to accurately analyze. Consequently, their widths were between 100 m and 4000 m, with a 100 m increment in the radius [41]. In so doing, enough samples for the regression analysis were obtained with only a minor computation burden in ArcGIS. Then, the buffer function in GIS was used, and forty GIS data layers were constructed.

Every buffer showed one buffer zone around the high AOD center. For each one, the proportions and areas of the five land use types were extracted using ArcGIS software, and the area $S(r)$ of each land use type was calculated as follows:

$$S(r) = C \times r^{D_r} \tag{3}$$

where r is the radius of buffer; C is a coefficient; and D_r is the radius dimension. The D_r of a certain land use type estimates the change in density from the high AOD center to its edge. Natural logarithms are used to simplify Eq. (3) as follows:

$$\ln S(r) = \ln C + D_r \times \ln r \tag{4}$$

When $D_r < 2$, for a certain land use type, the spatial density decreases nonlinearly from the high AOD center to its edge, and a smaller value indicates a faster decrease. Conversely, when $D_r > 2$, it implies that the spatial density increases from the high AOD center to its edge. Specially, when $D_r = 2$, the spatial density remains unchanged from the high AOD center to the edge. In conclusion, as the value of D_r decreases, the aggregation degree increases.

2.6 Contribution of AOD patterns for each land use type

To further quantify the impacts of different land use types on the AOD, their contributions to air pollution are constructed. Its definition is similar to the concept applied in the study of Chen et al. [42], which aims to estimate the contribution of each land use to a geographical phenomenon. First, the AODs were calculated to reflect the difference in air pollution patterns between spring and autumn, which was performed in Section 2.3. Next, the mean AODs of each land use type and the total landscape were calculated. When calculating the mean AODs for each land use type, all other land use types were masked out as background. Subsequently, the dT_i was imported into the calculation. It was the mean AOD difference for the corresponding land use type to mean AOD for the entire study extent of all images. The equation of dT_i is as follow:

$$dT_i = Mean\left(\Delta\ AOD_i\right) / Mean\ AOD \tag{5}$$

where $Mean\ AOD_i$ is the mean AOD difference of a given land use type; and $Mean\ AOD$ is the mean AOD over the entire study region of all images.

Second, S_i (%), the area proportion of each land use type, was extracted based on the classification in Section 2.2, respectively. Finally, multiplying Eq. (5) by S_i means that the contribution is defined as:

$$C_i = S_i \times dT_i \tag{6}$$

The greater the value of the contribution indicates a greater impact of the given land use change on AOD patterns.

3 Results and discussion

3.1 Relationship between the AOD patterns and landscape metrics

A correlation analysis between AOD and landscape metrics is processed to reflect the effects of landscape variations on AOD patterns. The class-based and landscape-based correlation coefficients are given in Table 3 and Table 4, respectively. For cropland, the variations between spring and autumn have different effects on the AOD variation, whereas for the other land uses, there are no significant differences because these land use types barely have variations in distribution. The AOD of bare land is not related to any of the landscape metrics, which maybe result from its 0.89% area proportion in spring and 0.60% area proportion in autumn. Thus, the seasonal variations in the urban green pattern influence the AOD spatial pattern. For the landscape-based metrics, the mean AOD positively correlates with PD, ED and SHDI but negatively correlates with LPI and CONTAG for both in spring and autumn, which indicates that the variations in landscape structure play a significant role in AOD variations.

Previous studies on air pollution patterns focused primarily on the effects of land use variations [2, 21, 43]. In agreement with our results, Borrego et al. [4] documented that mixed land use types provide better air quality. The present study shows that AOD variations are affected by not only land use composition but also its spatial configuration. Air pollution variations are correlated with various landscape pattern metrics (Tables 3 and 4). Air pollution is generally positively related to ED at both pixel-by-pixel and landscape scale (Table 3) and to PD and SHDI at the landscape scale (Table 4), suggesting that a mixture of built-up areas with urban green space and water reduces the AOD.

3.2 AOD variation in different land use types

As we know the climate factors have effects on air pollution [21]. In the autumn and winter, the air pollutants are unable to diffuse to upper air because it is easy to form an inversion layer in atmosphere. Therefore, Wuhan's air quality is more serious in autumn and winter. In addition, air quality begins to improve in spring because of the interaction effect between warm air and cold air. Their interaction contributes to winds and continuous rainy weather. During the summer, the effects of mid-latitude westerlies circulation and subtropical anticyclone lead to the significant increase of heavy rain. Thereafter, the air quality is better than other seasons [44, 45]. In spite of the impacts of climate factors, the main sources of atmospheric pollutants in Wuhan are combustion of coal, road traffic, metallurgy industries and secondary aerosol. Zhu et al. [45] reported that those air pollutant sources occupied 87% in the whole sources. In summary, the air pollutant sources in Wuhan are mainly different human activities and natural activities in different land use.

Fig. 6 and Fig. 7 show that there are high correlations between the logarithm of area with the logarithm of radius for these five land use types in spring and in autumn ($p < 0.001$). The slope of the fitted line is the radius dimension for every land use type. The slope implies that the radius dimension calculated by Eq. 4 is feasible to quantitatively analyze the change in land use intensity from the high urban AOD center to the outer boundary. For a certain land use type, its spatial density is nonlinearly decreasing (D_r<2) or nonlinearly increasing (D_r>2) or remains unchanged (D_r=2). In the fractal analysis, the forest yields the highest radius dimension, followed by water, cropland, built-up area and bare land in spring. In addition, the forest yields the highest radius dimension, followed by water, cropland, bare land and built-up area in autumn. Among these five land use types, the radius dimension of the built-up area is less than 2 and its D_r has smaller values in spring than in autumn. This result indicates that the density of the built-up area obviously decreases away from the high

AOD centers and the built-up area is the main contributor to air pollution. It is mainly due to high energy use, increases in traffic, an increase in the ground level fugitive dust, the clustering industrial activities, high population density and low air flushing rates [46]. This contribution is much more significant in spring than in autumn. The D_r of bare land is less than 2 in spring but close to 2 in autumn images, which may be caused by its small spatial extent and dispersed distribution. It is interesting to note that the radius dimension of cropland is greater than 2 (2.209) in late spring, whereas it is less than 2 (1.999) in mid-autumn, which results from an abrupt change of cropland from full coverage of the ground to unplanted. In combining field investigations with remote sensing images, it can be found that there are abundant areas of active vegetation and cropland in late spring; however, most of the croplands in Wuhan are already harvested, and at the same time, the forest content was low in mid-autumn. This corresponds with the results from the Wuhan Statistical Bureau [47].

During periods of high wind speed, cropland has been related to increases in air pollution in the vicinity of cropland fields [48]. Our analysis demonstrates that soil particles of unplanted and semi-bare croplands easily become airborne under the impact of wind. Aneja et al. [49] reported that agricultural activities played an important role in air pollution. However, there was no further study to analyze the different effects of seasonal agricultural activities on air pollution. In this paper, these impacts of agricultural activities were studied quantitatively in spring and autumn using a fractal analysis. In addition, the radius dimensions of water and forest are greater than 2 in both spring and autumn, and the D_r of forest was much more than the D_r of water, which indicates that the densities of water and forest increase away from the high AOD centers. These results correspond with the findings of Escobedo and Nowak [20] and Alonso et al. [50], who found that forest played an important role in reducing air pollutants. Salbu and Steinnes [51] reported that the increase in atmospheric moisture could promote the wet deposition of air pollutants and the absorption of aerosol particles. Urban water could greatly increase atmospheric moisture and reduce air pollution. Unfortunately, there are few known studies that quantitatively analyze the effects of water in reducing air pollution. In that study, a fractal analysis was used to study the impacts of land use on AOD patterns quantitatively, including water. It found that water and forest, especially forest, have negative contribution to air pollution.

3.3 Relationship between land use changes and AOD patterns

To further quantitatively assess the impacts of land use on AOD patterns, the mean AOD differences between each land use type to the mean regional AOD were calculated. By utilizing this information, an estimate of how land use changes may have contributed to the regional air pollution can be determined. Assuming the regional mean AOD was the long-term mean AOD in spring and autumn of the study area, the contribution of each land use type to the regional AOD can be computed. Similarly, the regional mean AODs based on 2010, 2011 2012 and 2013 HJ-1B images were calculated. Table 5 lists the regional mean AOD adjusted to changes in land use types based on several scenarios. It shows that there is a close connection between the changes in the AOD and the land use pattern.

Cropland has the highest contribution to the regional AOD, followed by built-up area, water, bare land and forest in spring, 2013. On the other hand, water has the highest contribution, followed by built-up area, forest, cropland and bare land in autumn, 2013. Among these land use types, the contributions of bare land (0.006 in spring and 0.001 in autumn) and built-up area (0.043 in spring and 0.034 in autumn) increase the AOD in both spring and autumn. This indicates that bare land and built-up area are the main contributors to increases in regional air pollution and these positive contributions are much more significant in spring. Although bare land has a small spatial extent, it is still an important contributor to the AOD as a result of its significant influence on regional AOD variation. This is because its dT are at their maximum in spring (0.73), and the third largest is in autumn (0.13). Forest and water have negative contributions to the AOD. These findings are in agreement with some earlier reports [52-55]. In addition, there is an interesting find for cropland, in that it has negative effect on the AOD in spring, whereas it has a positive effect in autumn in 2010, 2011, 2012 and 2013 (Table 5). In Wuhan, the cropland areas include summer crops (23.3%), kharif before Oct. 12 (39.2%) and kharif after Oct. 12 (14.8%) [47]. Given that vegetables are planted all year round, approximate 60.9% of cropland areas are exuberant crops in May and the others are young crops, whereas in October, 37.5% of cropland areas are young crops and the others are mainly unplanted. By analyzing the Wuhan Statistical Yearbook, we find that the vegetation coverage on May 11, 2013 is greater than that on Oct. 12, 2013. This results from seasonal variations and agricultural activities. In Wuhan, May is in the late spring, when young crops reach the exuberant crop stage and full coverage of the ground, whereas October is late in the harvesting season. The results suggest that agricultural activity is one of the major contributors to the seasonal variation of regional AOD, which is in agreement with the results found by Hays et al. [56]. Then, we further studied the different effects of seasonal agricultural activities on air pollution quantitatively. The result indicates the effect of land use change in the rise in the AOD mainly occurred in the built-up area, bare land and cropland, where large changes in land use occurred from 2010 to 2013 (Table 5). Our conclusion is that changes in the land use pattern can bring significant changes in the AOD. Human activity, including urban expansion, the intensification of agriculture, and fire management can further change natural landscapes.

4 Conclusions

The present study has sought to outline the major effects of land use type and structure variations on the AOD by performing landscape metrics analysis, fractal analysis and contribution analysis successively. The results obtained illustrate the significance of suitable land use planning for air pollution mitigation. It is evident that there are strong seasonality effects of land use variations on AOD patterns. Among the land use types, forest and water have negative effect on the deterioration of air pollution, whereas the urban areas and bare land have an increasing effect on air pollution. It is interesting to note the special status of cropland, which reduces air pollution in spring and tends to increase air pollution in autumn, which results from different types of farming operation. Although cropland is not a large contributor to the AOD per unit area, it still becomes a crucial contributor because of its large spatial extent and large area change. Quantitative studies on the effects of landscape structure variations on AOD patterns will enable us to better understand the processes involved in the effects of land use variations on the AOD for policy making and land use planning.

Acknowledgments

This work was financially supported by the National Natural Science of Foundation of China (41202136, 41571314), the Postdoctoral Science Foundation of China (2014M550513), and the Natural Science Basic Research Plan in the Shaanxi Province of China (2012JQ5010).

References

1. M. Agrawal, B. Singh, M. Rajput, F. Marshall and J. N. B. Bell, *Environ. Pollut.*, 2003, **126**, 323-329.
2. Q. Weng and S. Yang, *Environ. Monit. Assess.*, 2006, **117**, 463-489.
3. L. O. Marquez and N. C. Smith, *Environ. Modell. Software*, 1999, **14**, 541-548.
4. J. L. He, Y. Zha, J. H. Zhang, J. Gao and Q. Wang, *Adv. Space Res.*, 2014, **53**, 1337-1346.
5. G. Han, W. Gong, J. H. Quan, J. Li and M. Zhang, *Environ. Sci.-Process Impacts*, 2014, **16**, 916-923.
6. S. Ramachandran and R. Srivastava, *Environ. Sci.-Process Impacts*, 2013, **15**, 1070-1077.
7. X. Hu, L. A. Waller, A. Lyapustin, Y. Wang, M. Z. Al-Hamdan, W. L. Crosson, M. G. Estes Jr, S. M. Estes, D. A. Quattrochi, S. J. Puttaswamy and Y. Liu, *Remote Sens. Environ.*, 2014, **140**, 220-232.
8. A. Kumar, *Atmos. Environ.*, 2014, **83**, 291-300.
9. I. Kloog, P. Koutrakis, B. A. Coull, H. J. Lee and J. Schwartz, *Atmos. Environ.*, 2011, **45**, 6267-6275.
10. Y. J. Kaufman, D. Tanré, L. A. Remer, E. F. Vermote, A. Chu and B. N. Holben, *J. Geophys. Res. Atmos.*, 1997, **102**, 17051-17067.
11. Z. Wang, Q. Li, Q. Wang, S. Li, L. Chen, C. Zhou, L. Zhang and Y. Xu, *Journal of Remote Sensing*, 2012, **16**, 596-610.
12. L. Mei, Y. Xue, G. de Leeuw, T. Holzer-Popp, J. Guang, Y. Li, L. Yang, H. Xu, X. Xu, C. Li, Y.

Wang, C. Wu, T. Hou, X. He, J. Liu, J. Dong and Z. Chen, *Atmos. Chem. Phys.*, 2012, **12**, 9167-9185.

13. C. Y. Zhou, Q. H. Liu, B. Zhong, L. Sun and X. Z. Xin, 2009. In Geoscience and Remote Sensing Symposium, 2009 IEEE International, IGARSS 2009, 12-17 July 2009, pp V-413-V-416.
14. Y. Li, Y. Xue, X. He and J. Guang, *Atmos. Environ.*, 2012, **46**, 173-180.
15. Z. Wang, L. Chen, H. Gong and H. Gao, *Journal of Remote Sensing*, 2009, **13**, 1047-1059.
16. C. K. Chan and X. Yao, *Atmos. Environ.*, 2008, **42**, 1-42.
17. J. L. He, Y. Zha, J. H. Zhang and J. Gao, *Remote Sens.*, 2014, **6**, 1587-1604.
18. H. Romero, M. Ihl, A. Rivera, P. Zalazar and P. Azocar, *Atmos. Environ.*, 1999, **33**, 4039-4047.
19. G. Schaufler, B. Kitzler, A. Schindlbacher, U. Skiba, M. Sutton and S. Zechmeister-Boltenstern, *Eur. J. Soil Sci.*, 2010, **61**, 683-696.
20. F. J. Escobedo and D. J. Nowak, *Landscape Urban Plan.*, 2009, **90**, 102-110.
21. S. D. Superczynski and S. A. Christopher, *Remote Sens.*, 2011, **3**, 2552-2567.
22. K. De Ridder, F. Lefebre, S. Adriaensen, U. Arnold, W. Beckroege, C. Bronner, O. Damsgaard, I. Dostal, J. Dufek and J. Hirsch, *Atmos. Environ.*, 2008, **42**, 7059-7069.
23. J. G. Wu, W. J. Shen, W. Z. Sun and P. T. Tueller, *Landsc. Ecol.*, 2002, **17**, 761-782.
24. F. Herzog and A. Lausch, *Environ. Monit. Assess.*, 2001, **72**, 37-50.
25. J. Geoghegan, L. A. Wainger and N. E. Bockstael, *Ecol. Econ.*, 1997, **23**, 251-264.
26. J. G. Wu, G. D. Jenerette, A. Buyantuyev and C. L. Redman, *Ecol. Complex.*, 2011, **8**, 1-8.
27. M. C. Neel, K. McGarigal and S. A. Cushman, *Landsc. Ecol.*, 2004, **19**, 435-455.
28. Y. Zhang, Z. H. Liu, Y. Q. Wang, Z. X. Ye and L. Leng, *Remote Sens.*, 2014, **6**, 8760-8778.
29. Y. J. Kaufman, A. E. Wald, L. A. Remer, G. Bo-Cai, L. Rong-Rong and L. Flynn, *IEEE Trans. Geosci. Remote Sens.*, 1997, **35**, 1286-1298.
30. E. F. Vermote, D. Tanre, J. L. Deuze, M. Herman and J. J. Morcrette, *IEEE Trans. Geosci. Remote Sens.*, 1997, **35**, 675-686.
31. Q. Wang, Z. T. Wang, Q. Li, C. Y. Zhou, L. J. Zhang, Z. F. Wang, H. Q. Mao, X. Yang, H. Chen, L. X. Huang and W. J. Duan, 2011, CN 102103204 A (in Chinese).
32. Z. Li, X. Li, Y. Wang, A. Ma and J. Wang, *Int. J. Remote Sens.*, 2004, **25**, 5691-5703.
33. F. Bateni, S. Fakheran and A. Soffianian, *Environ. Monit. Assess.*, 2013, **185**, 10511-10519.
34. K. C. Seto and M. Fragkias, *Landsc. Ecol.*, 2005, **20**, 871-888.
35. F. Aguilera, L. M. Valenzuela and A. Botequilha-Leitão, *Landsc. Urban Plan.*, 2011, **99**, 226-238.
36. K. Riva-Murray, R. Riemann, P. Murdoch, J. M. Fischer and R. Brightbill, *Landsc. Ecol.*, 2010, **25**, 1489-1503.
37. A. B. Leitao and J. Ahern, *Landsc. Urban Plan.*, 2002, **59**, 65-93.
38. K. McGarigal, S. A. Cushman, M. C. Neel and E. Ene, 2002, DOI: citeulike-article-id:287784.
39. P. Frankhauser and R. Sadler, Hilliges, M., Ed.; University of Stuttgart: Stuttgart, Germany, 1991, DOI: 10.2307/1534622, pp. 57-65
40. R. White and G. Engelen, *Environment and planning A*, 1993, **25**, 1175–1199.
41. H. Wu, L. P. Ye, W. Z. Shi and K. C. Clarke, *Int. J. Appl. Earth Obs.*, 2014, 67-78.
42. X. L. Chen, H. M. Zhao, P. X. Li and Z. Y. Yin, *Remote Sens. Environ.*, 2006, **104**, 133-146.
43. M. Mohan, L. Dagar and B. R. Gurjar, *Environ. Monit. Assess.*, 2007, **130**, 323-339.
44. H. B. Li, Q. Yu and J. J. Shen, *Industrial Safety and Environmental Protection*, 2007, **33**,

46-48 (in Chinese).

45. Z. C. Zhu, L. L. Kong and K. Xia, *Environmental science & technology*, 2009, **32**, 64-67 (in Chinese).
46. S. Wang, J. Xing, S. Chatani, J. Hao, Z. Klimont, J. Cofala and M. Amann, *Atmos. Environ.*, 2011, **45**, 6347-6358.
47. Wuhan Statistical Bureau, *China Statistics Press, Beijing*, 2013 (in Chinese).
48. J. Kasumba, B. A. Holmén, A. Hiscox, J. Wang and D. Miller., *Atmos. Environ.*, 2011, **45**, 1668-1674.
49. V. P. Aneja, W. H. Schlesinger and J. W. Erisman, *Environ. Sci. Technol.*, 2009, **43**, 4234-4240.
50. R. Alonso, M. G. Vivanco, I. Gonzalez-Fernandez, V. Bermejo, I. Palomino, J. L. Garrido, S. Elvira, P. Salvador and B. Artinano, *Environ. Pollut.*, 2011, **159**, 2138-2147.
51. B. Salbu and E. Steinnes, *Trace elements in natural waters*, Springer Science & Business, 1995.
52. D. J. Nowak and D. E. Crane, 2000, 714-720.
53. K. Civerolo, G. Sistla, S. Rao and D. Nowak, *Atmos. Environ.*, 2000, **34**, 1615-1621.
54. K. P. Beckett, P. Freer-Smith and G. Taylor, *Environ. Pollut.*, 1998, **99**, 347-360.
55. J. Zhao, S. Chen, H. Wang, Y. Ren, K. Du, W. Xu, H. Zheng and B. Jiang, *Environ. Pollut.*, 2012, **167**, 148-154.
56. M. D. Hays, P. M. Fine, C. D. Geron, M. J. Kleeman and B. K. Gullett, *Atmos. Environ.*, 2005, **39**, 6747-6764.

Table 1. Band information of HJ-1B satellite.

Sensor	Band	Spectral range (μm)	Spatial resolution (m)	Amplitude Width (km)
CCD	1	0.43 - 0.52	30	360 (single) 700 (double)
	2	0.52 - 0.60		
	3	0.63 - 0.69		
	4	0.76 - 0.90		
IRS	1	0.75 - 1.10	150	720
	2	1.55 - 1.75		
	3	3.50 - 3.90		
	4	10.5 - 12.5	300	

Table 2. List of FRAGSTATS metrics.

Landscape metrics (abbreviation)	Definition (unit)	Calculation
Percentage of landscape (PLAND)	The proportion abundance of total area occupied by the corresponding land use type (%)	$PLAND = P_i = \frac{\sum_{j=1}^{n} a_{ij}}{A} \times 100$
Patch density (PD)	The number of patches per square kilometer of the corresponding land use type divided by total landscape area (n/km^2)	$PD = \frac{n_i \times 10000}{A} \times 100$
Largest patch index (LPI)	The percent of total landscape area contained by the largest patch (%)	$LPI = \frac{\max_{j=1}^{n}(a_{ij})}{A} \times 100$
Edge density (ED)	The total of length of all edge segments per hectare (m/ha)	$ED = \frac{\sum_{k=1}^{m} e_{ik}}{A} \times 10000$
Landscape shape index (LSI)	The sum of the lengths divided by the square standard of the total area	$LSI = \frac{0.25 \sum_{k=1}^{m} e_{ik}'}{\sqrt{A}}$
Clumpiness (CLUMPY)	The frequency with different pairs of corresponding patch type	$CLUMPY = \begin{bmatrix} \frac{G_i - P_i}{P_i} \, for G_i < P_i \,\&\, P_i < 5, else \\ \frac{G_i - P_i}{1 - P_i} \end{bmatrix}$
Contagion index (CONTAG)	Description of the landscape heterogeneity (%)	$CONTAG = \left\{ 1 + \frac{\sum_{i=1}^{m}\sum_{k=1}^{m}\left[P_i * (g_{ik} / \sum_{k=1}^{m} g_{ik})\right] * \left[\ln\left(P_i * (g_{ik} / \sum_{k=1}^{m} g_{ik})\right)\right]}{2\ln(m)} \right\} * 100$
Shannon's diversity index (SHDI)	A popular measure of the diversity in landscape	$SHDI = -\sum_{i=1}^{m}\left(P_i * \ln P_i\right)$

Table 3. Pearson correlation coefficients between mean AOD and class-level landscape pattern metrics.

Land use	Season	PLAND	PD	LPI	ED	LSI	CLUMPY
Built-up	Spring	.684**	-.018	.624**	.449*	-.303	-.088
	Autumn	.695**	-.138	.560**	.693**	.080	.114
Water	Spring	-.288	-.013	-.312	-.129	.171	-.380
	Autumn	-.281	.255	-.287	.199	.485*	.302
Forest	Spring	.210	.234	.153	.257	.184	.442
	Autumn	-.076	-.027	-.085	-.084	-.009	-.260
Cropland	Spring	-.647**	.726**	-.619**	.500**	.678**	-.600**
	Autumn	-.171	.474**	-.238	.212	.167	-.109
Bare	Spring	.196	.046	.247	.138	.028	.305
land	Autumn	.402	.531	-.026	.513	.535	-.013

*Correlation is significant at the 0.05 level (2-tailed).

**Correlation is significant at the 0.01 level (2-tailed).

Table 4. Pearson correlation coefficients between mean AOD and landscape-level landscape pattern metrics.

Image date	PD	LPI	ED	CONTAG	SHDI
Spring	.404*	-.358	.482*	-.494*	.586**
Autumn	.433*	-.211	.422*	-.144	.519**

*Correlation is significant at the 0.05 level (2-tailed).

**Correlation is significant at the 0.01 level (2-tailed).

507 **Table 5. Contribution of air pollution from all five land use types to the total**
508 **regional pollution.**

Land use	Season	dT_i	S_i (2010)	C_i	S_i (2011)	C_i	S_i (2012)	C_i	S_i (2013)	C_i
Built-up	Spring	0.17	19.82	0.034	23.11	0.039	24.50	0.042	25.39	0.043
	Autumn	0.13	20.24	0.026	23.98	0.031	25.31	0.032	27.03	0.034
Water	Spring	-0.21	14.62	-0.031	16.09	-0.034	15.07	-0.032	13.64	-0.029
	Autumn	-0.41	14.32	-0.058	15.93	-0.065	14.89	-0.061	14.43	-0.059
Forest	Spring	-0.04	1.32	-0.001	1.33	-0.001	1.31	-0.001	1.25	-0.001
	Autumn	-0.58	1.48	-0.009	1.46	-0.008	2.10	-0.012	1.91	-0.011
Cropland	Spring	-0.10	63.50	-0.065	59.21	-0.061	58.12	-0.060	58.83	-0.061
	Autumn	0.01	63.01	0.003	57.62	0.003	56.70	0.003	56.03	0.003
Bare land	Spring	0.73	0.74	0.005	0.26	0.002	1.00	0.007	0.89	0.006
	Autumn	0.13	0.95	0.001	1.01	0.001	1.00	0.001	0.60	0.001

509 **Fig. 1. Location of the study area.**

510

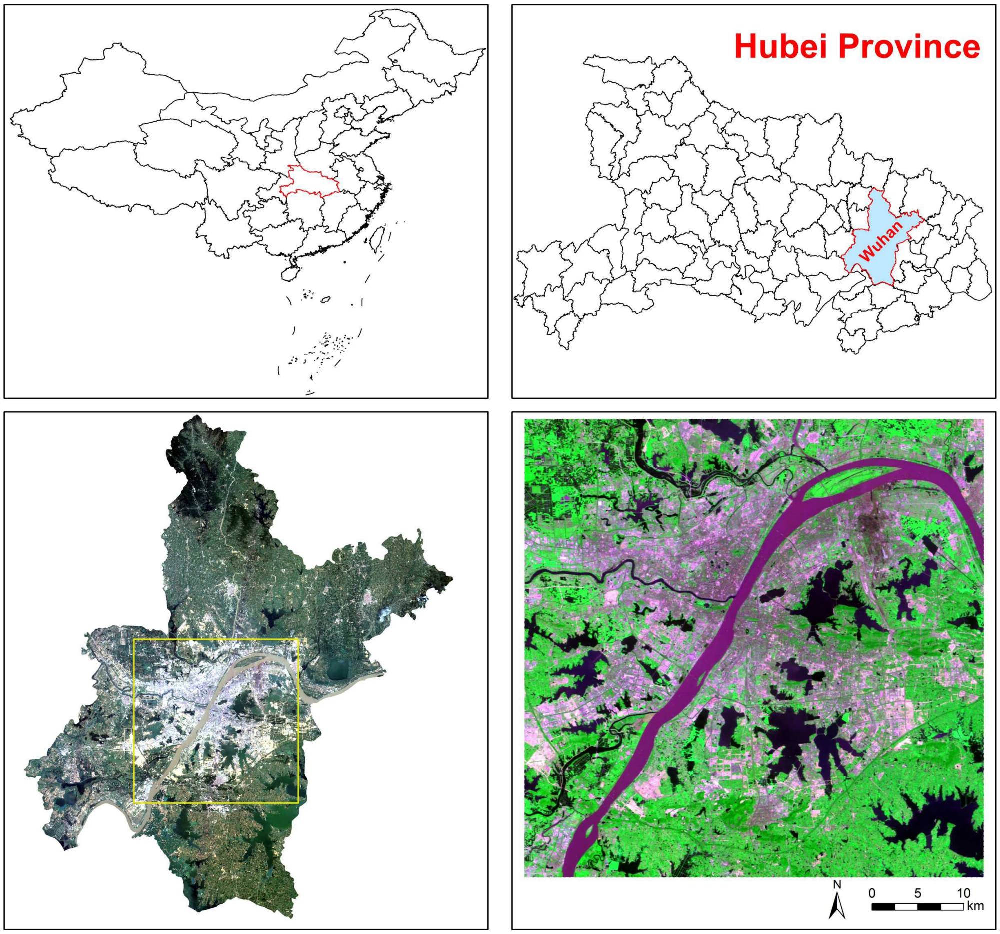

Fig. 2. The general framework of the assessment of AOD patterns.

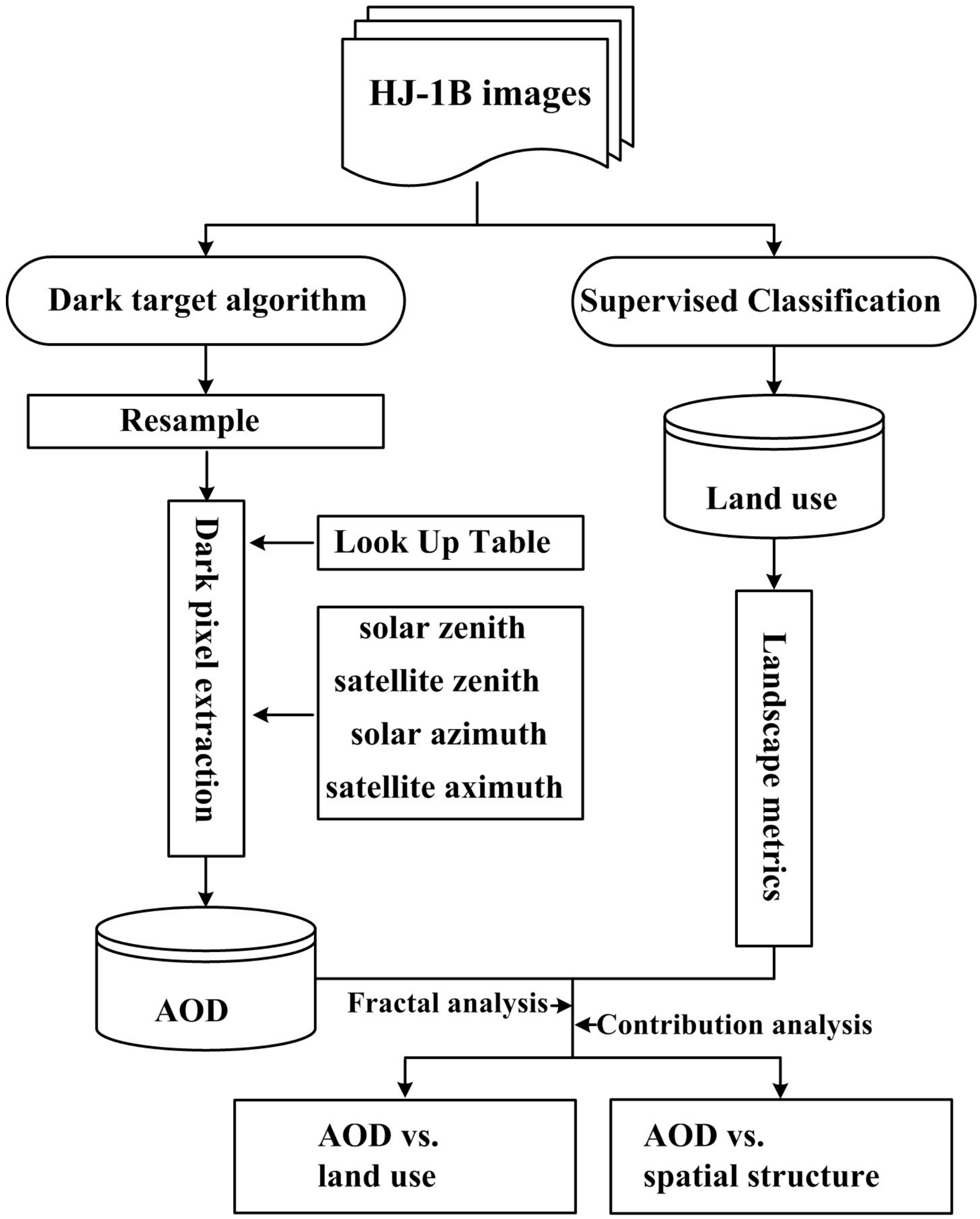

Fig. 3. Land use map for the study area on two dates: a: May 11, 2013; b: Oct. 12, 2013.

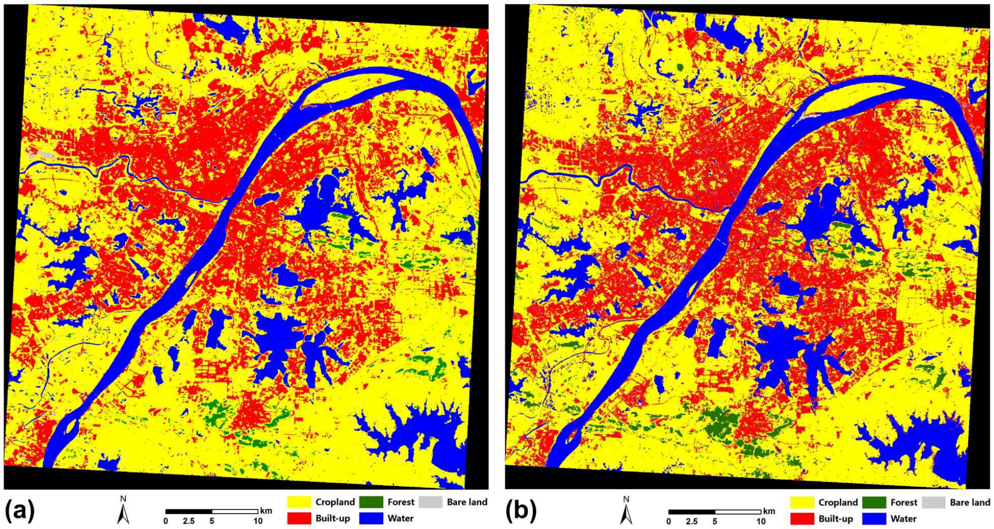

Fig. 4. Mean AOD maps for the study area on two seasons: a: Spring 2013; b: Autumn 2013.

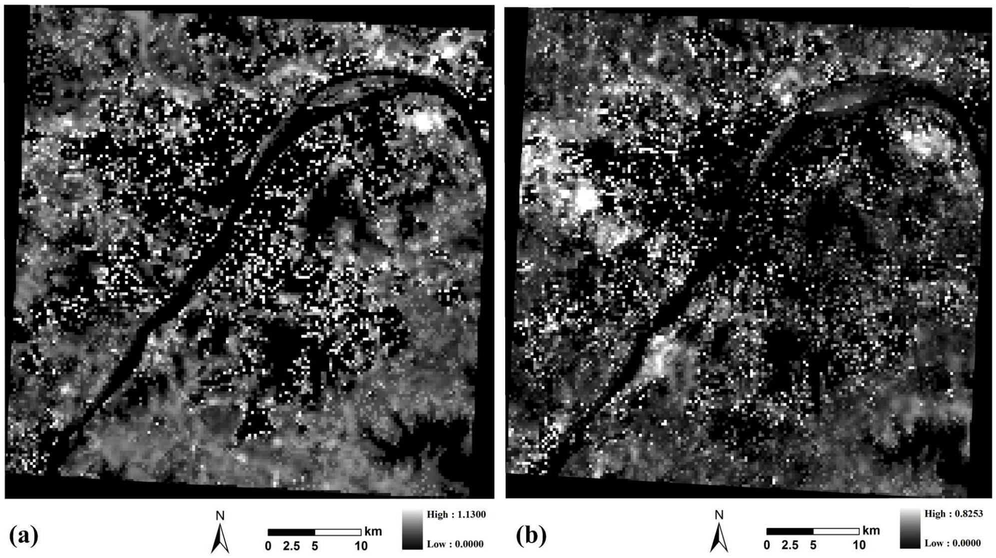

Fig. 5. Distribution map of high AOD centers for the study area on two seasons: a: Spring 2013; b: Autumn 2013.

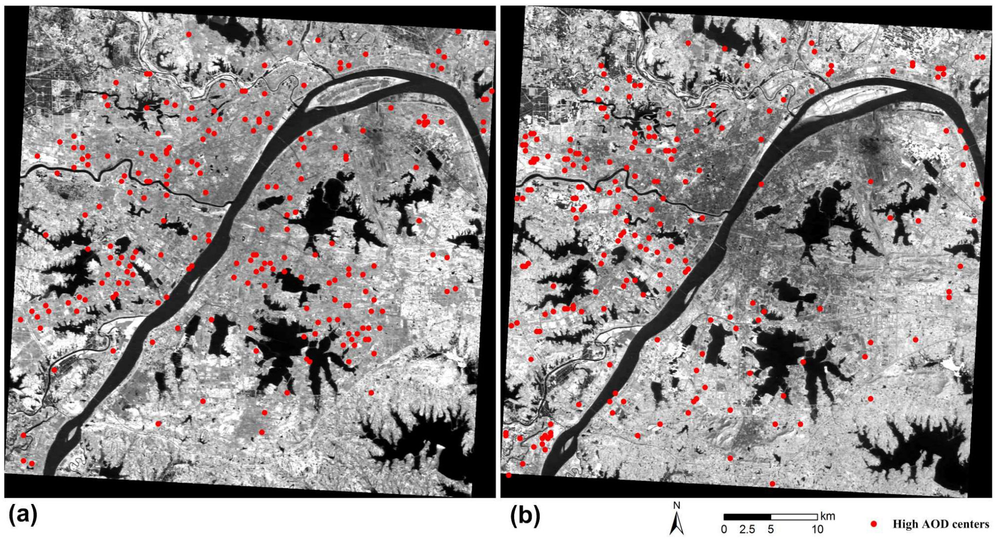

Fig. 6. lnS(r)-lnr scatter plot of the five land use types of Wuhan in spring.

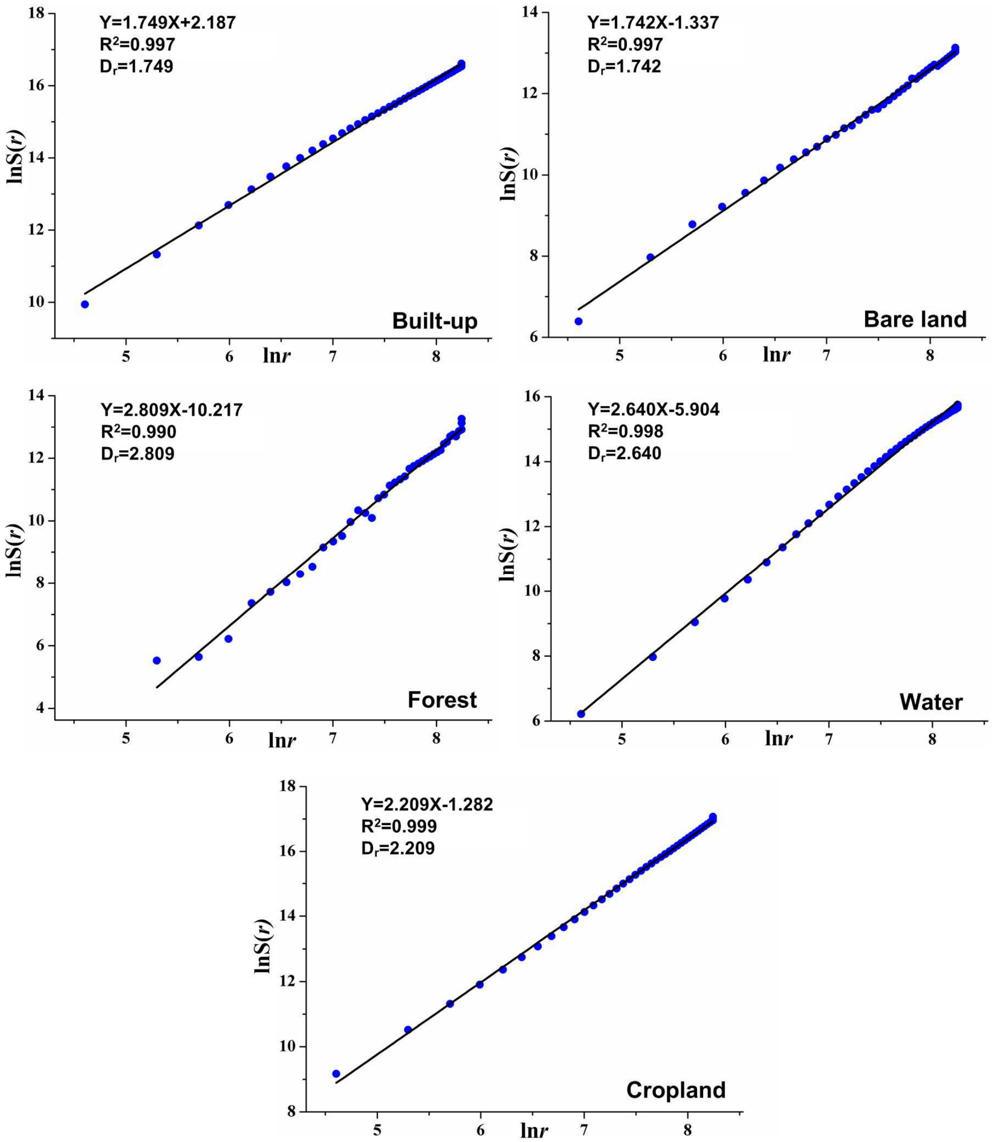

Fig. 7. lnS(r)-lnr scatter plot of the five land use types of Wuhan in autumn.